Collisional shift and broadening of the transition lines in pionic helium

Boyan Obreshkov and Dimitar Bakalov
Institute for Nuclear Research and Nuclear Energy, Bulgarian Academy of Sciences, Tsarigradsko chausseé 72, Sofia 1784, Bulgaria
(Received 16 April 2016; published 8 June 2016)

We calculate the density shift and broadening of selected dipole transition lines of pionic helium in gaseous helium at low temperatures up to $T = 12$ K and pressure up to a few bars. In the approximation of binary collisions the shift and broadening depend linearly on the density; we evaluate the slope of this linear dependence for a few spectral lines of known experimental interest and also investigate its temperature dependence. We find a blueshift of the resonance frequencies of the $(n,l) = (16,15) \to (16,14)$, $(17,16) \to (17,15)$, and $(16,15) \to (17,14)$ unfavored transitions and a redshift for the favored one, $(17,16) \to (16,15)$. The results are intended to significantly increase the efficiency of the laser spectroscopy investigations of pionic helium and help with the interpretation of the experimental data.

DOI: 10.1103/PhysRevA.93.062505

I. INTRODUCTION

Pionic helium is a three-body system composed of a helium nucleus, an electron in a ground state, and a π^- in a highly excited Rydberg state with principal quantum number $n \sim (m^*/m_e)^{1/2} \approx 16$, where m_e is the electron mass and m^* is the reduced mass of π^- and the helium nucleus. These states promptly deexcite via Auger transitions to lower-lying states which have large overlap with the helium nucleus and subsequently undergo fast nuclear absorption for times less than a picosecond. However, a small fraction of long-lived π^- have been observed in bubble-chamber experiments [1]. To explain this anomaly, Condo [2] suggested that metastable atomic states of π^- are formed in the reaction

$$\mathrm{He} + \pi^- \to [\mathrm{He}^+\pi^-]_{nl} + e^-, \tag{1}$$

in which the π^- occupies states with high angular momentum quantum number $l \sim n - 1 \approx 15$. These Rydberg states are expected to retain nanosecond-scale lifetimes against nuclear absorption and the electroweak decay $\pi^- \to \mu^- + \bar{\nu}_\mu$ with a lifetime of $\tau_{\pi^-} \approx 26$ ns. This is because in the nearly circular states of $\mathrm{He}^+\pi^-$ the overlap of the pion with the helium nucleus is minimized, whereas radiative deexcitation and the decay via Auger transitions which subsequently lead to fast nuclear absorption are strongly suppressed. An indirect confirmation of Condo's hypothesis has been obtained at TRIUMF [3] in experiments with π^- stopped in liquid helium; it has been found that about 2% of the pions retain a lifetime of 7 ns. A method for laser spectroscopy of metastable pionic helium atoms in gaseous helium has been proposed [4,5]. When comparing experimental transition frequencies to three-body QED calculations of pionic helium, the π^- mass can be determined with a fractional precision better than 10^{-6}. However, systematic effects such as collision-induced shift and broadening (S&B) of the transition lines, as well as the quenching of the metastable states, can prevent the experiment from achieving this high precision. Thus a reliable theoretical calculation for the density-dependent shift and width is needed for the extrapolation of transition wavelengths at zero target density.

II. COLLISIONAL SHIFT AND BROADENING OF THE TRANSITION LINES

A. Prerequisites: The potential energy surface

The collisional shift and broadening of the laser stimulated transition line $(n,l) \to (n',l')$ in pionic helium are obtained in the impact approximation of the binary collision theory of the spectral line shape [6–8].

This approach has already been applied in the calculations of the density effects on the line shape in antiprotonic helium [9–11] and produced theoretical results in agreement with experiment [12] (see also [13] and references therein).

The success of these calculations was due to the use of a highly accurate three-electron potential energy surface (PES) for the description of the binary interaction of an exotic helium atom with the atoms of the helium gas. The PES was evaluated with *ab initio* quantum chemistry methods [14] for nearly 400 configurations of the three heavy constituents of the interacting atoms (two helium nuclei and an antiproton or pion), selected to match the typical interpaticle distances in the experimentally interesting metastable states of exotic helium [15].

The configurations were parameterized with the length r of the vector joining the heavy particles in the antiprotonic or pionic atom, the length R of the vector joining its center of mass with the nucleus of the ordinary helium atom, and the angle θ between them.

Subsequently, the numerical values of the PES at these ~400 grid points were fitted with smooth functions $V(r,R,\theta)$. Two such fits, referred to as D47 and HN1, have been widely used in calculations; they have been shown to produce numerical results for the S&B in antiprotonic helium that differ by less than the overall numerical uncertainty.

Earlier attempts to use the same PES in the evaluation of the S&B of the spectral lines in pionic helium failed [15] because the typical distances r between the pion and the helium nucleus in the pionic helium metastable states are outside the range for which the PES has been calculated, and the two fits D47 and HN1 produce wrong values when used for extrapolation of the PES. In the present work we carefully analyzed the behavior of these fits and established that the problem can be resolved by appropriately truncating the integration over r in the expression for the effective state-dependent interatomic potentials in terms of $V(r,R,\theta)$ and the pionic helium atom

wave function $\chi_{nl}(r)$,

$$V_{nl}(R) = \frac{1}{2}\int_0^\infty dr \int d\theta \sin\theta \chi_{nl}^2(r) V(r,R,\theta) \;\rightarrow\; V_{nl}(R)$$
$$= \frac{1}{2}\int_{r_1}^{r_2} dr \int d\theta \sin\theta \chi_{nl}^2(r) V(r,R,\theta), \qquad (2)$$

while keeping under control at each step the induced numerical uncertainties; the optimal values of the truncating parameters were found to be $r_1 = 0.2$ a.u., $r_2 = 1.3$ a.u. The S&B of the four transition lines in pionic helium of experimental interest [4,16] were then evaluated by two alternative methods. Similar to the calculation of the S&B in antiprotonic helium [10], the obtained results differ by up to 30% and should be regarded as boundaries of the intervals of uncertainty of the theoretical values of the density shift and broadening slopes in pionic helium.

B. Impact approximation

In this approximation, the slope of the density and temperature-dependent collisional broadening $\Gamma_{fi}(T)$ and shift $\omega_{fi}(T)$ are given by [7]

$$\alpha_{fi}(T) = \frac{\partial \Gamma_{fi}(T)}{\partial N} = \left\langle \frac{\pi}{Mk} \sum_{L=0}^{\infty} (2L+1) 2\sin^2 \eta_{fi,L}(k) \right\rangle_T \qquad (3)$$

and

$$\beta_{fi}(T) = \frac{\partial \omega_{fi}(T)}{\partial N} = -\left\langle \frac{\pi}{Mk} \sum_{L=0}^{\infty} (2L+1) \sin 2\eta_{fi,L}(k) \right\rangle_T, \qquad (4)$$

respectively, where N denotes the number density of the target gas, the labels i and f stand for the set of quantum numbers of the initial and final pionic atom states n,l and $n'l'$, and $\langle\cdot\rangle_T$ denotes the thermal average over the Maxwell distribution. Both α and β are expressed in terms of the relative phase shifts

$$\eta_{fi,L}(k) = \delta_{iL}(k) - \delta_{fL}(k). \qquad (5)$$

The partial wave phases $\delta_L(k) = \delta_L(k, R \to \infty)$ are obtained from the asymptotic solution of the variable phase equation [17]

$$\frac{d}{dR}\delta_{nlL}(k,R) = -\frac{2MV_{nl}(R)}{k}[\cos\delta_{nlL}(k,R) j_L(kR)$$
$$- \sin\delta_{nlL}(k,R) n_L(kR)]^2, \qquad (6)$$

subject to the boundary condition $\delta_{nlL}(k,0) = 0$, where $k = \sqrt{2ME}$ is the wave number of relative motion for a given total collision energy E, M is the reduced mass of the collision system, $\{j_L(z), n_L(z)\}$ are the Riccati-Bessel functions, and $V_{nl}(R)$ is defined in (2).

In Figs. 1(a) and 1(b) we show the scattering phase shifts $\eta_L(k)$ for the "favored" transition $(17,16) \to (16,15)$ and for the "unfavored" one $(16,15) \to (16,14)$, respectively. For the unfavored transition in Fig. 1(a), the scattering phases are negative and are appreciably more than $-\pi/2$ over the entire range of wave numbers, giving rise to a blueshift of the transition frequency. For $k < 0.5$, the scattering of s,p, and d-waves gives the dominant contribution to the dipole transition line shape. A larger number of partial waves is required to converge the line shift and width with the increased wave number k. When $k \geqslant 1$, $\eta_L(k)$ exhibits a linear dependence on the wave number, showing that in this regime the effective potentials act as repulsive hard spheres with effective state-dependent radii and all phase shifts would tend to zero in the high-energy limit with $k \gg 1$. Since the phase shifts are small $|\eta_L| \ll \pi/2$ over the whole range of wave numbers, the collisional broadening of the transition line is negligible $\alpha \sim \sum_L (2L+1)\eta_L^2$ compared to the line shift $\beta \sim -\sum_L (2L+1)\eta_L$. In contrast the scattering phases are positive for the favored transition shown in Fig. 1(b), resulting in a redshift of the line center because $\eta_L(k) < \pi/2$ for $k > 0.1$ a.u. Since the s-wave scattering phase shift $\eta_0 \to \pi$ near $k \to 0$, the effective potential in the initial state $V_{17,16}(R)$ supports a single bound state through the Levinson theorem. Since the contribution of s-wave scattering becomes dominant towards the threshold, this bound state dramatically affects the transition line shape at very low speeds with $k < 0.1$ as the center frequency undergoes a blueshift when $\eta_0 > \pi/2$. However, the thermally averaged shift and width are weakly

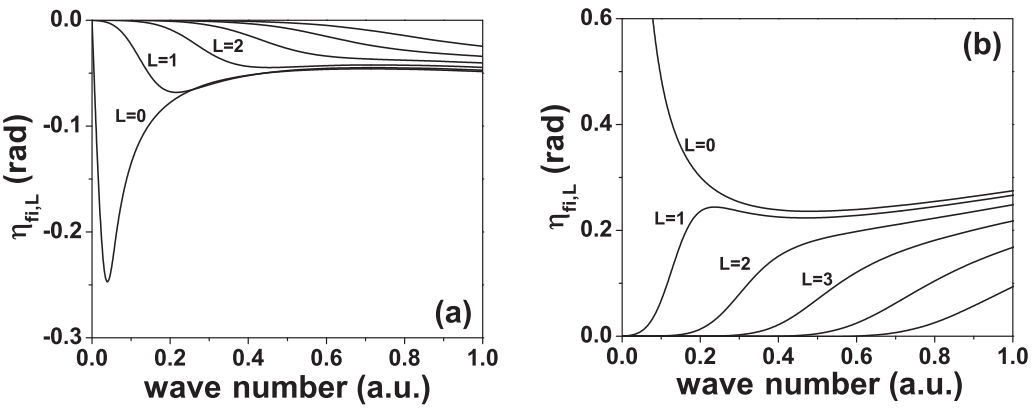

FIG. 1. The relative phase shifts $\eta_{fi,L}$ of Eq. (5) for (a) the unfavored laser-stimulated dipole transition $(16,15) \to (16,14)$ in pionic helium in gaseous helium and (b) the favored dipole transition $(17,16) \to (16,15)$. The different curves are labeled by the orbital angular momentum L.

TABLE I. Slope of the density shift and broadening are listed in the form $\beta(T)\,(\alpha(T))$ for selected transition lines in pionic helium and temperatures T in the range 4–12 K, in units 10^{-21} GHz cm^3. Listed are the numerical values obtained with Baranger's method while accounting for the anisotropic part of the potential energy surface [Eq. (7)] and in the approximation of central interatomic potentials [Eqs. (3) and (4)], as well as with Anderson's method [Eq. (12)], using either fit HN1 or D47 of the potential energy surface. The favored transition $(17,16) \rightarrow (16,15)$ is redshifted, while all the unfavored transitions undergo a blue density-dependent shift.

		Eq. (7)	Eqs. (3) and (4)		Eq. (12)	
Transition	T (K)	HN1	HN1	D47	HN1	D47
$(17,16) \rightarrow (16,15)$	4	−7.86(1.74)	−7.75(1.67)	−7.45(1.55)	−8.33(1.68)	−8.02(1.56)
	6	−7.95(1.63)	−7.84(1.52)	−7.55(1.41)	−8.61(1.74)	−8.30(1.62)
	8	−8.15(1.64)	−8.06(1.53)	−7.78(1.43)	−8.93(1.81)	−8.58(1.69)
	10	−8.35(1.68)	−8.28(1.57)	−8.00(1.47)	−9.18(1.88)	−8.84(1.75)
	12	−8.57(1.72)	−8.50(1.62)	−8.23(1.52)	−9.48(1.95)	−9.10(1.82)
$(17,16) \rightarrow (17,15)$	4	6.48(0.85)	6.27(0.75)	6.41(0.78)	4.43(0.36)	4.70(0.40)
	6	6.35(0.77)	6.16(0.66)	6.00(0.68)	4.52(0.34)	4.78(0.37)
	8	6.20(0.73)	6.04(0.63)	6.16(0.64)	4.62(0.33)	4.83(0.35)
	10	6.04(0.66)	5.92(0.58)	6.04(0.59)	4.65(0.31)	4.88(0.33)
	12	5.93(0.60)	5.82(0.53)	5.94(0.54)	4.75(0.32)	4.93(0.32)
$(16,15) \rightarrow (16,14)$	4	2.56(0.13)	2.53(0.12)	2.97(0.16)	2.07(0.08)	2.54(0.11)
	6	2.53(0.11)	2.54(0.10)	2.93(0.14)	2.11(0.07)	2.58(0.10)
	8	2.54(0.10)	2.52(0.10)	2.92(0.13)	2.16(0.07)	2.63(0.10)
	10	2.56(0.10)	2.51(0.09)	2.93(0.12)	2.21(0.07)	2.66(0.09)
	12	2.58(0.10)	2.53(0.09)	2.94(0.11)	2.24(0.30)	2.69(0.09)
$(16,15) \rightarrow (17,14)$	4	17.84(8.91)	17.69(7.94)	17.60(7.74)	11.37(2.66)	11.82(2.84)
	6	18.04(8.38)	18.10(7.41)	18.01(7.19)	11.74(2.63)	12.19(2.78)
	8	17.90(7.97)	18.06(7.22)	17.99(6.98)	12.11(2.64)	12.56(2.78)
	10	17.91(7.52)	18.04(6.92)	17.99(6.68)	12.45(2.67)	12.84(2.76)
	12	18.08(7.18)	18.17(6.67)	18.12(6.42)	12.70(2.68)	13.11(2.76)

affected by the low-velocity tail in the Maxwell distribution, for instance, at $T = 6$ K, $\beta \approx -7\times10^{-21}$ GHz cm^3, and $\alpha \approx 10^{-21}$ GHz cm^3.

The thermally averaged shift and width of the spectral lines for the selected transitions in pionic helium, obtained with the fits HN1 and D47, are given in the fourth and fifth columns of Table I, respectively. The temperature dependence of the line profile is relatively weak in gaseous helium. At low perturber density $N = 10^{21}$ cm^{-3}, we find a blueshift of the resonance frequencies for the $(n,l) = (16,15) \rightarrow (16,14)$, $(17,16) \rightarrow (17,15)$, and $(16,15) \rightarrow (17,14)$ transitions, $\beta = 2.5$, 6, and 18 GHz, respectively. For the favored transition $(17,16) \rightarrow (16,15)$, the line center is redshifted by 8 GHz. Thus in the absence of shape resonances in the potential scattering, the direction of the shift reflects the sign of the difference potential $\Delta V(R) = V_i(R) - V_f(R)$. The comparison of the corresponding linewidths in Table I makes evident that the spectral line for the unfavored transition $(16,15) \rightarrow (16,14)$ is only weakly affected by collisions since it is broadened by 0.1 GHz, which makes it suitable for spectroscopic measurements in pionic helium.

To further analyze the effect of the interaction energy $V(r,R,\theta)$ in the $He^+\pi^-$-He collision system, in Figs. 2(a) and 2(b) we plot the effective state-dependent potentials for the transitions $(17,16) \rightarrow (16,15)$ and $(16,15) \rightarrow (16,14)$, respectively, together with the difference potentials $\Delta V(R)$. Figures 2(c) and 2(d) present the corresponding variable phase functions at thermal collision energy with $T = 6$ K. For both transitions, the elastic scattering of s and p waves gives the dominant contribution to the line shift and width. The d-wave scattering is less efficient, and contributions of partial waves with $L \geqslant 3$ are suppressed due to a large centrifugal barrier. Figures 2(c) and 2(d) make evident that a substantial part of the line shift comes from the classically forbidden regions for relative motion with $4 \leqslant R \leqslant 5$ a.u. The s- and p-wave variable phases rise steeply in the classically allowed part of the scattering potentials $R > 5$ a.u., attain maxima near $R \approx 6$ a.u., then slightly fall off and saturate in the asymptotic region with $R > 7$ a.u. Thus the principal parts of the line shift and width at thermal collision energies are due to short-range binary encounters; the effect of the long-range van der Waals tail $V(R) \sim C_6/R^6$ acts as a weak perturbation.

C. Coupled partial waves

As an independent test of our hypothesis that the dominant contributions to the line shift and width are induced by effective central state-dependent scattering potentials in both initial and final states, we included the effect of the anisotropic part of the interaction energy. The collision-induced shift and broadening of the transition line shapes are evaluated from [18],

$$\alpha_{fi} + i\beta_{fi} = \sum_{JJ'LL'} (-1)^{L+L'}(2J+1)(2J'+1) \times \begin{Bmatrix} J' & J & 1 \\ l & l' & L \end{Bmatrix} \begin{Bmatrix} J' & J & 1 \\ l & l' & L' \end{Bmatrix} \times \left\langle \frac{\pi}{Mk}\left[\delta_{LL'} - S^{J}_{iL,iL'}(k) S^{J',*}_{fL,fL'}(k)\right] \right\rangle_T , \quad (7)$$

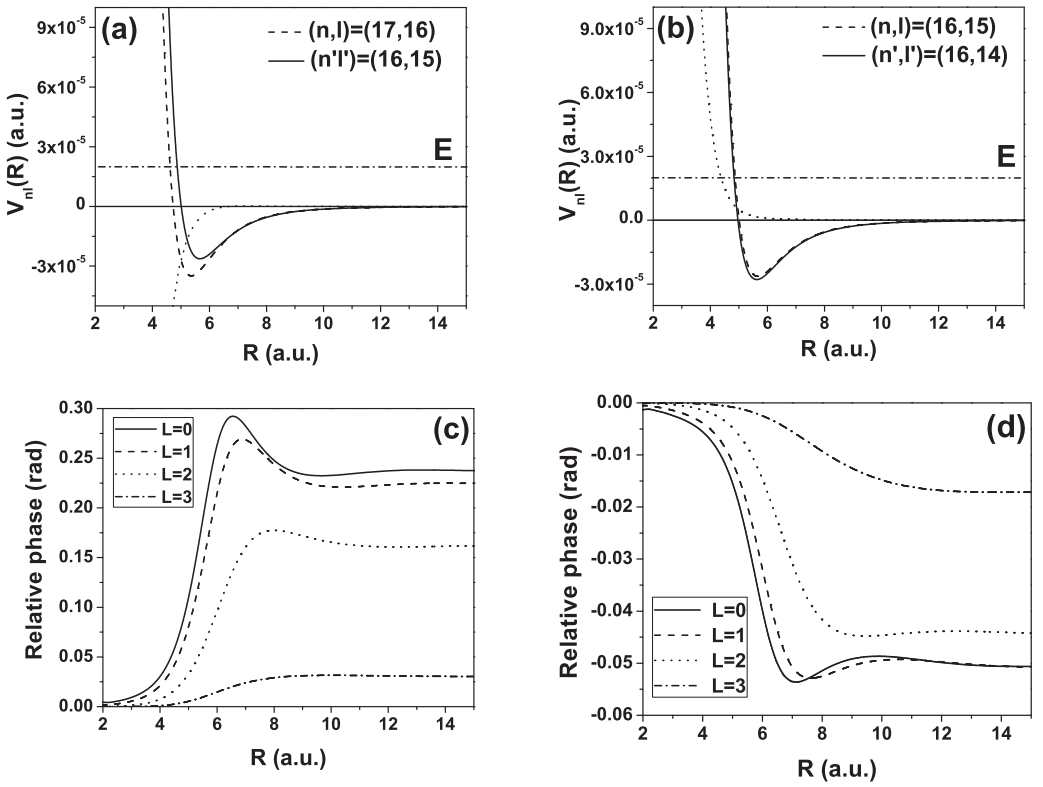

FIG. 2. (a) and (b) Potential-energy curves $V_{nl}(R)$ for the elastic scattering of pionic helium by an ordinary helium atom prior to (dashed line) and after (solid line) the absorption of a photon in the laser-stimulated dipole transitions (16,15) → (16,14) and (17,16) → (16,15), respectively. The potential energy difference $\Delta V = V_{nl} - V_{n'l'}$ is given by a dotted line, and the kinetic energy E of relative motion is indicated by the dash-dotted line. (c) and (d) Variable phase shifts (in radians) corresponding to the potential-energy curves in (a) and (b). The phase functions are labeled by the orbital angular momentum L.

where J and J' are the total angular momenta before and after the absorption of a photon.

We obtain the S-matrix elements $\mathbf{S}^J(k)$ from the asymptotic of the solutions of the coupled equations for the partial waves,

$$\frac{d\mathbf{S}^J(k,R)}{dR} = -i\frac{M}{k}[\mathbf{h}^{(2)}(kR) + \mathbf{S}^J(k,R)\cdot\mathbf{h}^{(1)}(kR)]\mathbf{V}^J(R) \times [\mathbf{h}^{(2)}(kR) + \mathbf{h}^{(1)}(kR)\cdot\mathbf{S}^J(k,R)],$$
$$\mathbf{S}^J(k) = \mathbf{S}^J(k,R\to\infty), \tag{8}$$

subject to the boundary condition $\mathbf{S}^J(k,0) = \mathbf{I}$, where $\mathbf{I}$ is the unit matrix and $\mathbf{h}^{(1)}(z)$ and $\mathbf{h}^{(2)}(z)$ are diagonal matrices of the Riccati-Hankel functions. We approximate the matrix representation of the interaction energy $V(\theta) = \sum_\lambda V_\lambda P_\lambda(\cos\theta)$ by truncating its Fourier expansion over Legendre polynomials at $\lambda = 2$, i.e.,

$$V^J_{nlL,nlL'}(R) \approx V_{nl}(R)\triangle(JlL)\delta_{LL'} + V^{(2)}_{nl}(R)\sqrt{(2l+1)(2L+1)}(-1)^{l+L'-J}C^{l0}_{l0,20} \times C^{L'0}_{L0,20}\begin{Bmatrix} 2 & L & L' \\ J & l & l \end{Bmatrix}, \tag{9}$$

where $C^{c\gamma}_{a\alpha,b\beta}$ are the Clebsch-Gordan coefficients, $\triangle(abc)$ imposes the triangle condition, and

$$V^{(2)}_{nl}(R) = \frac{5}{2}\int_{r_1}^{r_2} dr\,\chi^2_{nl}(r)\int d\theta\,\sin\theta\,V(r,R,\theta)P_2(\cos\theta). \tag{10}$$

At low-collision energies, the S matrix for the coupled s and d waves can be parameterized in terms of two variable phases δ^J_0 and δ^J_2 and a mixing angle ε^J,

$$\mathbf{S}^J(k,R) \approx \begin{pmatrix} e^{2i\delta^J_0(k,R)}\cos 2\varepsilon^J(k,R) & ie^{i[\delta^J_0(k,R)+\delta^J_2(k,R)]}\sin 2\varepsilon^J(k,R) \\ ie^{i[\delta^J_0(k,R)+\delta^J_2(k,R)]}\sin 2\varepsilon^J(k,R) & e^{2i\delta^J_2(k,R)}\cos 2\varepsilon^J(k,R) \end{pmatrix}. \tag{11}$$

In the $\varepsilon^J \to 0$ limit, the S matrix is diagonal, and the usual decoupled result is recovered. In Fig. 3 we plot the mixing angle ε^J as a function of the separation R between the colliding atoms at thermal energy with $T = 6$ K.

The principal effect of the weak quadrupole coupling is to facilitate scattering of d waves due to the s-wave admixture in both initial- and final-state wave functions. The enhancement of the d-wave elastic scattering is most effective in the

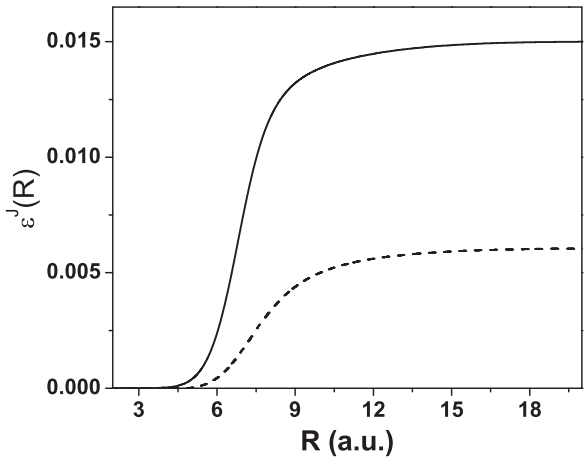

FIG. 3. Collision-induced mixing of s and d waves in the laser-stimulated dipole transition (17,16) → (16,15) in pionic helium in gaseous helium. The position dependence of the mixing angle $\varepsilon^J(R)$ prior to and after the photon absorption is given by the solid and dashed lines, respectively. The total angular momentum is $J = 16$ in the initial state and $J = 15$ in the final state. The collision energy corresponds to $T = 6$ K.

classically allowed region for both initial- and final-state motions, where the colliding atoms experience the attractive part of the scattering potential. The numerical results for the line shape obtained with the HN1 fit are given in the third column of Table I. As the comparison demonstrates, the anistropic pairwise interaction has a minor effect on the line shifts, which justifies our approximation of using central state-dependent potentials to describe the collision. However, the linewidths for certain transitions are noticeably affected by the quadrupole interaction; for example, the enhancement of d-wave scattering causes additional broadening of the transition line (16,15) → (17,14) by 1 GHz at low temperatures. In contrast the narrow line of the transition (16,15) → (16,14) is insensitive to anisotropic interatomic interactions.

D. Anderson's semiclassical method

The slopes of the shift and broadening of the spectral line of the transition can alternatively be represented in the form [9]

$$\alpha_{fi}(T)7 = \frac{\partial \Gamma_{fi}}{\partial N} = \mathrm{Re}\,\Phi, \quad \beta_{fi}(T) = \frac{\partial \omega_{fi}}{\partial N} = \mathrm{Im}\,\Phi,$$

$$\Phi = \left\langle 2\pi\, v_T \int db\, b \left[1 - \exp\left(-i \int dt\, (V_{n'l'}[|\mathbf{R}(t)|] - V_{nl}[|\mathbf{R}(t)|]) \right) \right] \right\rangle_T, \tag{12}$$

where $\mathbf{R}(t)$ is the trajectory of the *classical* relative motion of the pionic and ordinary helium atoms (i.e., the vector joining the positions of the atoms at time t), while b and $v_T = \sqrt{2kT/M}$ are the impact parameter and the initial velocity of the relative thermal motion of the colliding atoms outside the interatomic potential range.

Equation (12) in its initial form involving rectilinear trajectories $\mathbf{R}(t) = \mathbf{R}_0 + t\mathbf{v}_T$ was proposed by Anderson [19]; however, it fails to give reasonable estimates of the density effects at low temperature. The substantial modification that makes Eq. (12) applicable in this case is to use instead the curvilinear trajectories determined by the binary interaction potential in the *initial state* for the transition of interest, $V_{nl}(R)$, as suggested in [9,10]. The numerical results for the density shift and broadening slopes for the transition lines in pionic helium of experimental interest, obtained with fits HN1 and D47, are given in the sixth and seventh columns of Table I, respectively.

In agreement with the observations in Sec. II B, the detailed look at the multiple integral in Eq. (12) reveals that the dominant contribution to Φ (through the integrals of the difference $V_{n'l'}[R(t)] - V_{nl}[R(t)]$ along the various classical trajectories) comes from the range $4 \leqslant R \leqslant 10$ a.u. For the favored transition up to 95% of the value of Φ is accumulated in the range $4 \leqslant R \leqslant 6$ a.u., while for the unfavored transition the contributions from the domains $4 \leqslant R \leqslant 6$ and $6 \leqslant R \leqslant 10$ are balanced. This emphasizes once more the importance of using a realistic and accurate PES in the evaluation of the density effects; estimates based on the asymptotic shape of the interaction potentials, valid for $R > 10$ a.u., cannot be reliable.

III. NUMERICAL RESULTS AND DISCUSSION

The cumulative Table I presents the numerical results for the slopes of the density shift and broadening, $\beta_{fi}(T)$ and $\alpha_{fi}(T)$, of four transition lines in pionic helium of declared experimental interest, obtained with the theoretical methods outlined in the preceding section and using two different fits of the PES. We see that in some cases the numerical values differ quite significantly and require further comments.

(1) The two different fits HN1 and D47 produce values that differ by up to 20%. As pointed out, this is related to the extrapolation of the fits outside the range of configurations relevant in antiprotonic helium for which the PES was initially evaluated. As long as both fits give close results for antiprotonic helium, we have no reason to consider any of them as preferable; instead, the difference between the two values should be regarded as numerical uncertainty of the results that could only be eliminated with a new calculation of the PES for a wider range of configurations.

(2) The two theoretical approaches of Sec. II B and II D produce results that differ by only a few percent for the favored transition (17,16) → (16,15) and by up to one third for the unfavored ones. The good agreement with experiment of the results for antiprotonic helium based on the use of classical trajectories is not an argument to consider this approach as more credible in the case of pionic helium. We should therefore refer to these differences as a theoretical uncertainty of the results.

(3) Accounting for the contribution of the anisotropic part of the PES only slightly affects the shift slope $\beta_{fi}(T)$ and has a larger impact on the broadening slope $\alpha_{fi}(T)$, which is still much smaller than the theoretical uncertainty.

(4) The moderate temperature dependence of the results is uniformly reproduced in all the calculations.

IV. CONCLUSION

We have calculated the density shift and broadening of four dipole transition lines in pionic helium in gaseous helium. At thermal collision energies, we find a blueshift of the line center in the unfavored transitions $(n,l) = (16,15) \rightarrow (16,14)$, $(17,16) \rightarrow (17,15)$, and $(16,15) \rightarrow (17,14)$, while the transition frequency is redshifted for the favored transition $(17,16) \rightarrow (16,15)$. The narrow collisional line width (0.1 GHz) of the laser-induced resonance transition $(n,l) = (16,15) \rightarrow (16,14)$ makes it suitable for precision spectroscopy of pionic helium atoms. We demonstrate that the major part of the collisional shift and width of the spectral lines is induced by the short-range part of the interatomic potential. Our result may be helpful in the extrapolation of the transition wavelengths in pionic helium to zero density of the perturbing helium gas.

While the significant overall uncertainty of the S&B slopes may not allow for a direct extrapolation of the experimentally observed resonance frequencies of the laser-induced transitions to zero target gas density, we expect that knowing the density shift to $\sim$20% fractional accuracy will greatly enhance the efficiency of the precision laser spectroscopy study of pionic helium.

[1] J. G. Fetkovich and E. J. Pewitt, Phys. Rev. Lett. **11**, 290 (1963).
[2] G. T. Condo, Phys. Lett. **9**, 65 (1964).
[3] S. N. Nakamura, M. Iwasaki, H. Outa, R. S. Hayano, Y. Watanabe, T. Nagae, T. Yamazaki, H. Tada, T. Numao, Y. Kuno, and R. Kadono, Phys. Rev. A **45**, 6202 (1992).
[4] M. Hori, A. Söter, and V. I. Korobov, Phys. Rev. A **89**, 042515 (2014).
[5] M. Hori, A. Söter, H. Aghai-Kozhani, D. Barna, A. Dax, R. S. Hayano, Y. Murakami, and H. Yamada, Hyperfine Interact. **233**, 83 (2015).
[6] E. Lindholm, Ark. Mat. Astron. Fys. **28B**, 3 (1941).
[7] M. Baranger, Phys. Rev. **111**, 481 (1958).
[8] N. Allard and J. Kielkopf, Rev. Mod. Phys. **54**, 1103 (1992).
[9] D. Bakalov, B. Jeziorski, T. Korona, K. Szalewicz, and E. Tchukova, Phys. Rev. Lett. **84**, 2350 (2000).
[10] D. Bakalov, B. Jeziorski, T. Korona, B. Obreshkov, and K. Szalewicz (unpublished).
[11] D. Bakalov, Hyperfine Interact. **209**, 25 (2012).
[12] H. A. Torii *et al.*, Phys. Rev. A **53**, R1931 (1996).
[13] T. Yamazaki, N. Morita, R. Hayano, E. Widmann, and J. Eades, Phys. Rep. **366**, 183 (2002).
[14] B. Jeziorski and K. Szalewicz, in *Encyclopedia of Computational Chemistry*, edited by P. von Ragué Schleyer, N. L. Allinger, T. Clark, J. Gasteiger, P. A. Kollman, H. F. Schaefer, III, and P. R. Schreiner (Wiley, Chichester, UK, 1998), Vol. 2, p. 1376; B. Jeziorski, K. Szalewicz, and G. Chalasinski, Int. J. Quantum Chem. **14**, 271 (1978).
[15] D. Bakalov, Hyperfine Interact. **233**, 127 (2015).
[16] M. Hori (private communication).
[17] F. Calogero, *Variable Phase Approach to Potential Scattering* (Academic Press, New York, 1967).
[18] G. Peach, in *Springer Handbook of Atomic and Molecular Physics*, edited by G. Drake (Springer, New York, 2006), pp. 875–890.
[19] P. W. Anderson, Phys. Rev. **86**, 809 (1952).